Published in final edited form as:
Biochem Pharmacol. 2013 May 15; 85(10): . doi:10.1016/j.bcp.2013.02.030.

The insecticidal neurotoxin Aps III is an atypical knottin peptide that potently blocks insect voltage-gated sodium channels

Niraj S. Bende[a], **Eunji Kang**[b], **Volker Herzig**[a], **Frank Bosmans**[c,d], **Graham M. Nicholson**[b], **Mehdi Mobli**[a], and **Glenn F. King**[a,*]

[a]Institute for Molecular Bioscience, The University of Queensland, St Lucia, QLD 4072, Australia

[b]School of Medical & Molecular Biosciences, University of Technology, Sydney, Broadway NSW 2007, Australia

[c]Department of Physiology, Johns Hopkins University – School of Medicine, Baltimore MD 21205, USA

[d]Solomon H. Snyder Department of Neuroscience, Johns Hopkins University – School of Medicine, Baltimore MD 21205, USA

Abstract

One of the most potent insecticidal venom peptides described to date is Aps III from the venom of the trapdoor spider *Apomastus schlingeri*. Aps III is highly neurotoxic to lepidopteran crop pests, making it a promising candidate for bioinsecticide development. However, its disulfide-connectivity, three-dimensional structure, and mode of action have not been determined. Here we show that recombinant Aps III (rAps III) is an atypical knottin peptide; three of the disulfide bridges form a classical inhibitor cystine knot motif while the fourth disulfide acts as a molecular staple that restricts the flexibility of an unusually large β hairpin loop that often houses the pharmacophore in this class of toxins. We demonstrate that the irreversible paralysis induced in insects by rAps III results from a potent block of insect voltage-gated sodium channels. Channel block by rAps III is voltage-independent insofar as it occurs without significant alteration in the voltage-dependence of channel activation or steady-state inactivation. Thus, rAps III appears to be a pore blocker that plugs the outer vestibule of insect voltage-gated sodium channels. This mechanism of action contrasts strikingly with virtually all other sodium channel modulators isolated from spider venoms that act as gating modifiers by interacting with one or more of the four voltage-sensing domains of the channel.

Keywords

voltage-gated sodium channel; neurotoxin; spider-venom peptide; pore blocker; gating modifier; inhibitor cystine knot

*Address for correspondence: Prof. Glenn F. King, Institute for Molecular Bioscience, The University of Queensland, 306 Carmody Road, St Lucia, Queensland 4072, Australia; Phone: +61 7 3346-2025; Fax: +61 7 3346-2021; glenn.king@imb.uq.edu.au.

Conflict of interest
The authors declare that they have no conflicts of interest.

1. Introduction

Insects serve as vectors for a wide range of debilitating and potentially lethal human diseases such as malaria, dengue, Chagas disease, and yellow fever [1]. About 3.3 billion people, almost half of the world's population, are at risk of contracting vector-borne disease [2]. Moreover, despite intensive control measures, insect pests reduce world crop yields by 10–14% annually [3, 4].

Despite the widespread introduction of insect-resistant transgenic crops, chemical insecticides remain the dominant method for controlling insect pests in both the agricultural and public health arenas. These chemicals target a very small number of molecular targets in the insect nervous system [5]. As a result, their widespread use over several decades has promoted the evolution of resistant insect populations, with >600 insects and mites now resistant to one or more classes of chemical insecticides [6]. In addition, key classes of insecticides have been withdrawn from sale or their use has been restricted by regulatory authorities due to growing environmental and human health concerns [7]. Thus, there is an urgent need to develop novel classes of insecticides or alternative methods of insect pest control.

A promising approach in the agricultural sector is to engineer crops to produce insecticidal toxins. By 2010, 148 million hectares of genetically modified (GM) crops had been planted in 29 countries, representing 10% of all cropland [8]. While the introduction of GM crops that express *Bacillus thuringiensis* (*Bt*) toxins has provided an alternative and potentially safer method of insect control than chemical insecticides, alternative insect-toxin transgenes are urgently needed as constitutive expression of *Bt* toxin in transgenic plants is likely to expedite resistance development [9].

There are very few well characterised toxins that could be considered as alternatives or adjuncts to *Bt*. However, some of the most promising candidates are novel insecticidal peptides that have been isolated from the venom of spiders [7, 10–12], the most successful insect predators on the planet. Most of these peptides are highly stable because they contain an inhibitor cystine knot (ICK) motif [13, 14] that provides them with resistance to extremes of pH, high temperatures, and proteolytic enzymes [7, 15]. One of the first insecticidal spider-venom peptides to be reported was Aps III from the venom of the trapdoor spider *Apomastus schlingeri* [16]. With a reported LD_{50} of 133 pmol/g against the tobacco hornworm *Manduca sexta*, this peptide is one of the most potent insect toxins described to date according to ArachnoServer [17, 18]. Aps III comprises 37-residues with four disulfide-bonds, but its three-dimensional structure and mode of action are unknown.

Here we describe the development of an efficient *E. coli* expression system that was used to produce recombinant Aps III (rAps III) for functional and structural studies. The 3D solution structure of rAps III determined using NMR spectroscopy revealed an inhibitor cystine knot motif that is commonly found in spider-venom peptides. However, rAps III contains an additional disulfide bridge that is employed as a molecular staple to tie together the ends of a very large β-hairpin loop. We demonstrate that the insecticidal activity of rAps III results from a potent block of insect voltage-gated sodium (Na_v) channels in combination with a weaker block of insect voltage-gated calcium (Ca_v) channels. However, in striking contrast to previously characterised Na_v channel blockers from spiders, all of which are gating modifiers [19], rAps III appears to be a pore blocker that plugs the outer vestibule of insect Na_v channels.

2. Material and Methods

2.1 Chemicals

All chemicals were purchased from Sigma-Aldrich Australia (Castle Hill, NSW, Australia), Sigma-Aldrich USA (St Louis, MO, USA), or Merck Chemicals (Kilsyth, Victoria, Australia) with the exception of isopropyl-β-D-thiogalactopyranoside (IPTG) and streptomycin (Life Technologies, Victoria, Australia), tetrodotoxin (Alomone Labs, Israel), and HPLC-grade acetonitrile (RCI Labscan, Bangkok, Thailand). $^{13}C_6$-glucose and $^{15}NH_4Cl$ were from Sigma-Aldrich Australia. Recombinant His_6-TEV protease (EC 3.4.22.44) was produced in-house used a published protocol [20].

2.2 Production of recombinant Aps III

A synthetic gene encoding Aps III, with codons optimised for expression in *Escherichia coli*, was produced and cloned into a variant of the pLIC-MBP expression vector [21] by GeneArt (Invitrogen, Regensburg, Germany). This vector (pLIC-NSB1) encodes a MalE signal sequence for periplasmic export [22], a His_6 tag for affinity purification, a maltose binding protein (MBP) fusion tag to aid solubility [23], and a tobacco etch virus (TEV) protease recognition site directly preceding the codon-optimised Aps III gene (Fig. 1A).

The plasmid encoding Aps III was transformed into *E. coli* strain BL21(λDE3) for recombinant toxin production. Protein expression and purification were performed as described previously [24] with minor modifications. Briefly, cultures were grown in Terrific Broth at 37°C with shaking at 120 rpm. Toxin gene expression was induced with 1 mM IPTG at an OD_{600} of 1.1–1.2, then cells were grown at 18°C for a further 12 h before harvesting by centrifugation for 15 min at 8000 rpm. For production of uniformly $^{13}C/^{15}N$-labelled rAps III, cultures were grown in minimal medium supplemented with $^{13}C_6$-glucose and $^{15}NH_4Cl$ as the sole carbon and nitrogen sources, respectively.

The His_6-MBP-toxin fusion protein was extracted from the bacterial periplasm by cell disruption at 26 kPa (TS Series Cell Disrupter, Constant Systems Ltd, Northants, UK), then captured by passing the extract (buffered in 40 mM Tris, 500 mM NaCl, pH 8.0) over Ni-NTA Superflow resin (Qiagen). Proteins bound non-specifically were removed by washing with 10 mM imidazole then the fusion protein was eluted with 500 mM imidazole. The eluted fusion protein was concentrated to 10 ml and the buffer was exchanged to remove imidazole. Reduced and oxidised glutathione were then added to 0.6 mM and 0.4 mM, respectively, to maintain TEV protease activity and promote folding of the protein. Approximately 100 μg of His_6-tagged TEV protease was added per mg of rAps III, then the cleavage reaction was allowed to proceed at room temperature for 12 h. The cleaved His_6-MBP and His_6-TEV were removed by passing the solution over Ni-NTA Superflow resin, while the eluate containing rAps III was collected for further purification using reverse-phase HPLC (RP-HPLC). RP-HPLC was performed on a Vydac C18 column (250 × 4.6 mm, particle size 5 μm) using a flow rate of 1 ml/min and a gradient of 20–40% Solvent B (0.043% trifluoroacetic acid (TFA) in 90% acetonitrile) in Solvent A (0.05% TFA in water) over 20 min. rAps III contains a non-native N-terminal serine residue (a vestige of the TEV protease cleavage site), making it one-residue longer than native Aps III (Fig. 1B).

2.3 Mass spectrometry

Toxin masses were confirmed by matrix assisted laser desorption ionization–time of flight mass spectrometry (MALDI-TOF MS) using a Model 4700 Proteomics Bioanalyser (Applied Biosystems, CA, USA). RP-HPLC fractions were mixed (1:1 v:v) with α-cyano-4 hydroxy-cinnamic acid matrix (5 mg/ml in 50/50 acetonitrile/H_2O) and MALDI-TOF

spectra were acquired in positive reflector mode. All reported masses are for monoisotopic $[M+H]^+$ ions.

2.4 Insecticidal assays

rAps III dissolved in insect-saline [25] was injected into the ventro-lateral thoracic region of sheep blowflies (*Lucilia cuprina*; mass 19.7–23.9 mg) using a 1.0 ml Terumo Insulin syringe (B-D Ultra-Fine, Terumo Medical Corporation, MD, USA) with a fixed 29 G needle fitted to an Arnold hand micro-applicator (Burkard Manufacturing Co. Ltd., England). A maximum volume of 2 μl was injected per fly. Thereafter, flies were individually housed in 2 ml tubes and the paralytic activity was determined after 24 h. A total of three tests were carried out and for each test seven doses of rAps III (n = 10 flies per dose) and the appropriate control (insect saline; n = 30 flies each) were used. PD_{50} values were calculated as described previously [26].

2.5 Electrophysiological measurements

2.5.1 Primary cell culture—Dorsal unpaired median (DUM) neurons were isolated from unsexed adult American cockroaches (*Periplaneta americana*) as described previously [27, 28]. Briefly, terminal abdominal ganglia were removed and placed in normal insect saline (NIS) containing (in mM): NaCl 180, KCl 3.1, *N*-hydroxyethylpiperazine-*N*-ethanesulfonic acid (HEPES) 10 and D-glucose 20. Ganglia were then incubated in 1 mg/ml collagenase (type IA) (EC 3.4.24.3) for 40 min at 29°C. Following enzymatic treatment, ganglia were washed three times in NIS and triturated through a fire-polished Pasteur pipette. The resultant cell suspension was then distributed onto 12-mm diameter glass coverslips pre-coated with 2 mg/ml concanavalin A (type IV). DUM neurons were maintained in NIS supplemented with 5 mM $CaCl_2$, 4 mM $MgCl_2$, 5% foetal bovine serum and 1% penicillin and streptomycin, and maintained at 29°C, 100% humidity.

2.5.2 Patch-clamp electrophysiology—Ionic currents were recorded in voltage-clamp mode using the whole-cell patch-clamp technique employing version 10.2 of the pCLAMP data acquisition system (Molecular Devices, Sunnyvale, CA). Data were filtered at 5–10 kHz with a low-pass Bessel filter with leakage and capacitative currents subtracted using *P-P*/4 procedures. Digital sampling rates were set between 15 and 25 kHz depending of the length of the protocol. Single-use 0.8–2.5 MΩ electrodes were pulled from borosilicate glass and fire-polished prior to current recordings. Liquid junction potentials were calculated using JPCALC [29], and all data were compensated for these values. Cells were bathed in external solution through a continuous pressurised perfusion system at 1 ml/min, while toxin solutions were introduced via direct pressurised application via a perfusion needle at ~50 μl/min (Automate Scientific, San Francisco, CA) to a bath volume of 300 μl. To avoid issues of desensitization or rundown of currents, particularly with Ca_V channel currents, recording periods were kept as short as possible with the effect of toxin recorded within 5 min of control recordings. Control data was not acquired until at least 20 min after whole-cell configuration was achieved. This was to eliminate the influence of fast time-dependent shifts in steady-state inactivation resulting in current rundown, particularly when recording Na_V channel currents (I_{Na}). Time-dependent shifts in steady-state Na_V channel inactivation are typically of the order of 2–3 mV beyond this period and do not significantly influence current amplitude. Experiments were performed with a single concentration of toxin tested on one cell, which was subsequently repeated in separate experiments using unexposed cells. The number of independent recordings for each type of experiment is provided in the relevant sections of the results. All experiments were performed at ambient room temperature (20–23°C).

To record I_{Na}, the external bath solution contained (in mM): NaCl 80, CsCl 5, $CaCl_2$ 1.8, tetraethylammonium chloride (TEA-Cl) 50, 4-aminopyridine (4-AP) 5, HEPES 10, $NiCl_2$ 0.1, and $CdCl_2$ 1, adjusted to pH 7.4 with 1 M NaOH. The pipette solution contained (in mM): NaCl 34, CsF 135, $MgCl_2$ 1, HEPES 10, ethylene glycol-bis(2-aminoethylether)-*N*,*N*,*N*′,*N*′-tetraacetic acid (EGTA) 5, and ATP-Na_2 3, adjusted to pH 7.4 with 1 M CsOH. Due to the reported current rundown with calcium as a charge carrier [30], $BaCl_2$ replaced $CaCl_2$ in all experiments on voltage-activated calcium (Ca_V) channels.

The external bath solution for barium current (I_{Ba}) recordings contained (in mM): Na acetate 140, TEA-Br 30, $BaCl_2$ 3 and HEPES 10, adjusted to pH 7.4 with 1 M TEA-OH. The external solution also contained 300 nM tetrodotoxin (TTX) to block Na_V channels. Pipette solutions contained (in mM): Na acetate 10, CsCl 110, TEA-Br 50, ATP-Na_2 2, $CaCl_2$ 0.5, EGTA 10 and HEPES 10, adjusted to pH 7.4 with 1 M CsOH. The external bath solution for recording global voltage-activated potassium (K_V) channel currents (I_K) contained (in mM): NaCl 200, K gluconate 50, $CaCl_2$ 5, $MgCl_2$ 4, TTX 0.3, HEPES 10 and D-glucose 10, adjusted to pH 7.4 with 1 M NaOH. The pipette solution consisted of (in mM): K gluconate 135, KF 25, NaCl 9, $CaCl_2$ 0.1, $MgCl_2$ 1, EGTA 1, HEPES 10 and ATP-Na_2 3, adjusted to pH 7.4 with 1 M KOH.

To eliminate any influence of differences in osmotic pressure, all internal and external solutions were adjusted to 400 ± 5 mOsmol/l with sucrose. Experiments were rejected if there were large leak currents or currents showed signs of poor space clamping.

2.5.3 Curve-fitting and statistical analyses

Data were analysed using AXOGRAPH X version 1.3 (Molecular Devices). Curve-fitting of *I-V* data was performed using GraphPad Prism version 5.00d for Macintosh (GraphPad Software, San Diego). Comparisons of two sample means were made using a paired Student's *t*-test and differences were considered to be significant if $p < 0.05$. All data are presented as mean ± standard error of the mean (SEM) of *n* independent experiments.

Concentration-response curves were fitted using the following Logistic equation:

$$y = \frac{1}{1+([x]/IC_{50})^{n_H}} \quad \text{Equation 1}$$

where *x* is the toxin dose, n_H is the Hill coefficient (slope parameter), and IC_{50} is the median inhibitory concentration to block channel currents.

The following equation was employed to fit current-voltage (*I-V*) curves:

$$I = g_{max}\left(1 - \left(\frac{1}{1+\exp[(V - V_{1/2})/s]}\right)\right)(V - V_{rev}) \quad \text{Equation 2}$$

where *I* is the amplitude of the current at a given test potential *V*, g_{max} is the maximal conductance, $V_{1/2}$ is the voltage at half-maximal activation, *s* is the slope factor, and V_{rev} is the reversal potential.

The voltage dependence of steady-state Na_V channel inactivation (h_∞/V) data were normalised to the maximum peak current in the control or maximum peak current and fitted using the following Boltzmann equation:

$$h_\infty = \frac{A}{1+\exp[(V - V_{1/2})/k]} \quad \text{Equation 3}$$

where A is the fraction of control maximal peak I_{Na} (value of 1.0 under control conditions), $V_{1/2}$ is the midpoint of inactivation, k is the slope factor, and V is the prepulse voltage.

2.5.4 Two-electrode voltage-clamp recordings from *Xenopus* oocytes—To prepare cRNA for oocyte injection, separate plasmids encoding the α-subunit of the Na_V1 channel from the German cockroach *Blatella germanica* ($BgNa_V1$; [31]) and the *Drosophila* Na_V1 auxiliary subunit TipE [32] were linearised with *Not*I, followed by *in vitro* transcription using T7 polymerase (mMESSAGE mMACHINE kit, Life Technologies, CA, USA). After *Xenopus* oocytes were co-injected at 1:5 molar ratio with cRNA encoding $BgNa_V1$ and TipE, they were incubated for 2–3 days at 17°C (in 96 mM NaCl, 2 mM KCl, 5 mM HEPES, 1 mM $MgCl_2$, 1.8 mM $CaCl_2$, 50 μg/ml gentamycin, pH 7.6) prior to recording $BgNa_V1$-mediated currents via two-electrode voltage-clamp recording techniques using an OC-725C Oocyte Clamp Amplifier (Warner Instruments, CT, USA) with a 150-μl recording chamber. Data were filtered at 4 kHz and digitised at 50 kHz using pCLAMP 10. Microelectrode resistances were 0.1–1 MΩ when filled with 3 M KCl. The external recording solution contained (in mM): 96 NaCl, 2 KCl, 5 HEPES, 1 $MgCl_2$ and 1.8 $CaCl_2$, pH 7.6. Experiments were performed at ambient temperature (~22 °C) and leak and background conductance was subtracted by blocking the residual sodium current with TTX.

Voltage–activation relationships were obtained by measuring steady-state currents elicited by stepwise depolarisations of 5 mV from a holding potential of −90 mV and calculating conductance (G) using $G = I/(V_m–E_{rev})$ in which G is conductance, I is peak inward current, V_m is the test potential, and E_{rev} is the reversal potential. Reversal potentials were individually estimated for each data set [33]. After addition of the toxin to the recording chamber (150 μl), the equilibration between the toxin and the channel was monitored using weak depolarizations (50-ms test pulse to a voltage near the foot of the *G-V* curve, ~ −30 mV) elicited at intervals of 5 s. We recorded voltage–activation relationships in the absence and presence of toxin. Off-line data analysis was performed using Clampfit 10 (Molecular Devices, USA) and Origin 8 (OriginLab, MA, USA).

2.6 Structure determination

Recombinant $^{15}N/^{13}C$-labelled Aps III was dissolved in 20 mM sodium phosphate, pH 6.0 to a final concentration of 450 μM 5^2H_2O was added, then the sample was filtered using a low-protein-binding Ultrafree-MC centrifugal filter (0.22 μm pore size; Millipore, MA, USA) and 300 μL was added to a susceptibility matched 5 mm outer-diameter microtube (Shigemi Inc., Japan). NMR data were acquired at 25°C using a 900 MHz NMR spectrometer (Bruker BioSpin, Germany) equipped with a cryogenically cooled probe. 3D and 4D data used for resonance assignments were acquired using non-uniform sampling (NUS). Sampling schedules that approximated the signal decay in each indirect dimension were generated using sched3D [34]. NUS data were processed using the Rowland NMR toolkit (www.rowland.org/rnmrtk/toolkit.html) and maximum entropy parameters were automatically selected as previously described [35]. ^{13}C- and ^{15}N-edited HSQC-NOESY (mixing time of 200 ms) experiments were acquired using uniform sampling. All experiments were acquired in H_2O except for the ^{13}C-edited HSQC-NOESY, which was acquired in D_2O.

Dihedral angles (29 Φ, 30 ψ) were derived from TALOS+ chemical shift analysis [36] and the restraint range for structure calculations was set to twice the estimated standard

deviation. The Thr6–Pro7 peptide bond was determined to be in the *trans* conformation on the basis of characteristic NOEs and the C_α and C_β chemical shifts of the Pro residue.

Six backbone amide protons were identified as being involved in hydrogen-bonds by comparison of 2D ^{1}H-^{15}N HSQC spectra acquired either in H_2O or 60 min after reconstitution of lyophilised protein in D_2O. The presence of intense NOESY crosspeaks for the hydroxyl proton of Thr 4 indicated that it is also engaged in a hydrogen bond. Hydrogen-bond acceptors and disulfide-bond partners were identified from preliminary structure calculations, and hydrogen-bond and disulfide-bond restraints were applied in subsequent structure calculations as described previously [37]. NOESY spectra were manually peak picked and integrated, then peaklists were automatically assigned, distance restraints extracted, and an ensemble of structures calculated using the torsion angle dynamics package CYANA 3.0 [38]. The tolerances used for CYANA 3.0 were 0.025 ppm in the direct ^{1}H dimension, 0.03 ppm in the indirect ^{1}H dimension, and 0.3 ppm for the heteronucleus ($^{13}C/^{15}N$). During the automated NOESY assignment/structure calculation process, CYANA assigned ~86% of all NOESY crosspeaks (1127 out of 1313).

3. RESULTS

3.1 Production of recombinant Aps III

Recombinant production of venom toxins is often challenging due to the presence of multiple disulfide bonds, which cannot be formed in the cytoplasm of most prokaryotic and eukaryotic cells because of the reducing intracellular environment. An alternative approach that has proved successful for expression of disulfide-rich spider toxins [24, 39, 40] is production in the periplasm of *E. coli*, where the enzymes involved in disulfide-bond formation are located [41]. Thus, we attempted to produce rAps III using an IPTG-inducible construct (Fig. 1A) that allowed export of a His_6-MBP-toxin fusion protein to the *E. coli* periplasm.

Using this expression system, a significant amount of His_6-MBP-toxin fusion protein was recovered in the soluble cell fraction following IPTG induction (Fig. 1C, lanes 1–4). The fusion protein was subsequently purified using nickel affinity chromatography (Fig. 1C, lanes 5–8) then eluted from the column and cleaved with His_6-tagged TEV protease (Fig. 1C, lanes 9–10). The His_6-tagged MBP and TEV protease were removed by passage over a nickel column, then the eluted toxin was further purified using RP-HPLC (Fig. 1D). rAps III eluted as a single major disulfide-bond isomer with a retention time of ~25 min under the chosen experimental conditions. The purity of recombinant rAps III following RP-HPLC was >98% as assessed by SDS-PAGE and MALDI-TOF mass spectrometry (Fig. 1D, inset), and the final yield was ~1.5 mg of toxin per litre of culture.

3.2 rAps III induces irreversible paralysis in insects

The insecticidal activity of rAps III was tested using the blowfly *Lucilia cuprina*. This dipteran pest is the causative agent of flystrike, which results in annual economic losses in Australia of ~$280 million [42]. rAps III induced flaccid paralysis in adult *L. cuprina*, and the PD_{50} measured 24 h after injection was 700 ± 35 pmol/g (Fig. 1E). The toxicity assay used does not allow measurement of toxic effects for periods extending beyond 24 h as the survival rate in control cohorts begins to decrease, possibly due to confinement of the flies in small tubes. However, flies paralyzed by a high dose of rAps III did not recover but died two days post-injection. We conclude that rAps III produces an irreversible paralysis in blowflies and would most likely produce similar effects in related dipterans such as mosquitoes and tsetse flies that vector human diseases.

3.3 rAps III is a potent blocker of insect Na_V channels

The majority of insecticidal spider toxins that have been isolated to date modulate the activity of voltage-gated ion channels [7, 11, 28, 43, 44]. We therefore used patch-clamp electrophysiology to examine the ability of rAps III to modulate the activity of a variety of ion channels in cockroach DUM neurons.

Na_V channel currents (I_{Na}) in DUM neurons were elicited using 50-ms depolarising test pulses from a holding potential (V_h) of −90 mV to −10 mV every 10 s (0.1 Hz) (Fig. 2D). This elicited a rapidly activating and inactivating ionic current characteristic of classical I_{Na} observed previously in DUM neurons (Fig. 2A,B) [28, 45, 46]. This current was confirmed to be mediated by Na_V channels following complete I_{Na} inhibition with 300 nM TTX (Fig. 2B). In separate experiments, perfusion with rAps III produced a concentration-dependent inhibition of peak I_{Na}. This occurred in the absence of any significant changes in the time to peak, time course of inactivation (decay) kinetics, or time course of tail currents at the end of the depolarising test pulse, as shown in the representative current traces in Fig. 2A. At a concentration of 30 nM, rAps III reduced peak I_{Na} by 29 ± 6% (n = 5 cells, $p < 0.05$). In separate experiments, higher concentrations of 300 nM and 1 μM rAps III produced a concentration-dependent reduction in peak I_{Na} by 43 ± 5% (n = 9 cells, $p < 0.001$) and 53 ± 5% (n = 5 cells, $p < 0.01$), respectively.

The half-maximal inhibitory concentration (IC_{50}) for rAps III on DUM neuron I_{Na} was estimated to be ~540 nM (Fig. 2C). However, the Hill coefficient was significantly less than unity (shallower slope), which may reflect incomplete block at higher concentrations, as has been observed with certain μ-conotoxin derivatives [47].

3.4 rAps III is a classical pore blocker

To determine whether toxin inhibition of peak I_{Na} was due to a depolarising shift in the voltage dependence of activation, families of I_{Na} (Fig. 3A,B) were elicited using a test pulse that depolarised the cell from V_h of −90 mV to +70 mV for 50 ms in 10-mV increments (Fig. 3F). Peak I_{Na} were then normalised against the maximum peak I_{Na} in the control and plotted against membrane potential *(V)* to establish an I_{Na}-*V* curve. Peak I_{Na} was then fitted to Equation 2 (Materials and Methods) using non-linear regression analysis. In the absence of toxin, I_{Na} activated around −60 mV. This threshold did not shift in the presence of any concentration of rAps III tested as shown by the superimposed control and toxin curves around −60 mV (Fig. 3C,D). The voltage at half maximum Na_V channel activation ($V_{1/2}$) in control cells was only marginally shifted (4 mV) in the hyperpolarising direction in the presence of 1 μM rAps III (control $V_{1/2}$ = −35 ± 1 mV versus toxin $V_{1/2}$ = −31 ± 3 mV; n = 4 cells, $p < 0.005$). This is more clearly observed as a lack of any significant shift in the voltage dependence of activation when currents recorded in the presence of toxin were normalised to the peak inward control current (Fig. 3D). No significant shifts in $V_{1/2}$ were observed with either 30 nM or 300 nM rAps III. Considering the time-dependent hyperpolarising shifts in $V_{1/2}$ of around 5 mV over a 10−15 min period that occur in whole-cell patch clamp configurations, this would indicate that the toxin does not alter the voltage-dependence of activation. Importantly, only a depolarising shift in the voltage-dependence of Na_V channel activation would reduce $I_{Na.}$

To determine whether toxin-induced block of I_{Na} was voltage-dependent, peak I_{Na} in the presence of toxin was calculated as a fraction of the corresponding control I_{Na} from the I_{Na}-*V* relationships. Data were then fitted by linear regression and the slope coefficient determined. This revealed that the inhibition of Na_V channels by 1 μM rAps III was voltage-independent and the binding of the toxin to the channel was not relieved at increasing

membrane potentials (Fig. 3E). The slope of the line did not significantly deviate from zero ($p > 0.05$, $n = 4$ cells).

In separate experiments, the effects of rAps III on the voltage-dependence of steady-state inactivation (h_∞/V) were examined to determine whether the reduction of peak I_{Na} was due to stabilisation of the inactivated (closed) state of the channel, as opposed to a pore blocking mechanism. Accordingly, experiments were conducted using a two-pulse protocol consisting of a 1 s conditioning pre-pulse ($V_{prepulse}$) followed by a 50 ms test pulse (V_{test}) to −10 mV. The conditioning prepulse clamped the membrane potential from −120 mV to 0 mV in 10-mV increments (see inset to Fig. 4A,B). Due to increasing levels of depolarisation during the conditioning prepulse, channels eventually accrue in the inactivated state and have insufficient time to recover from inactivation before the test pulse. Thus, I_{Na} amplitude decreases with increasing prepulse potential (Fig. 4A,C). In the presence of 30 nM rAps III, I_{Na} was inhibited to 79 ± 3% ($n = 3$ cells) of control amplitude (parameter 'A' in Equation 3). Normalisation of the toxin data to the maximum peak I_{Na} during the test pulse revealed that the curves almost completely overlap (Fig. 4D) with an insignificant 2-mV hyperpolarising shift in h_∞/V from −56 ± mV in controls to −58 ± mV in the presence of rAps III ($p > 0.05$, $n = 3$ cells; Fig. 3D). Thus the 21% reduction in Na_V channel current does not appear to be the result of a reduction in channel availability due to stabilisation of the channels in the inactivated state. Therefore rAps III appears to be a classical pore blocker.

3.5 rAps III is a weak blocker of insect Ca_V channels

We next tested the ability of rAps III to modulate the activity of insect Ca_V channels as numerous spider-venom peptides have been demonstrated to inhibit this channel [48, 49]. Two distinct Ca_V channel subtypes have been previously observed in DUM neurons: mid to low-voltage-activated (M-LVA) and high-voltage activated (HVA) Ca_V channels [46]. M-LVA and HVA Ca_V channel barium currents (I_{Ba}) were elicited using alternating 100-ms depolarising test pulses to −30 mV (M-LVA I_{Ba}) and +20 mV (HVA I_{Ba}) from a V_h of −90 mV every 7 s. These elicited inward currents characteristic of classical I_{Ba} observed previously in DUM neurons [46]. Perfusion with 1 μM rAps III caused weak inhibition of both M-LVA and HVA Ca_V channel currents. This occurred in the absence of changes in M-LVA and HVA I_{Ba} activation and inactivation kinetics, with no alteration in the time to reach peak or timecourse of current decay (Fig. 5A). The M-LVA Ca_V channel currents were reduced by 28 ± 5% ($p < 0.01$, $n = 5$ cells) and HVA Ca_V channel currents by 31 ± 7% ($p < 0.01$, $n = 6$ cells). The small difference in the block between inhibition of M-LVA and HVA current was statistically insignificant (unpaired Student's *t*-test, $p > 0.05$). Given the weak effects on Ca_V channel currents at 1 μM rAps III, experiments were not conducted at 30 nM or 300 nM concentrations. In an additional smaller number of cells there was a partial recovery from Ca_V channel current inhibition. In these cells initial rapid inhibition was followed by partial recovery to a steady-state level. This resulted in a statistically insignificant block of both M-LVA Ca_V channel currents (18 ± 6% block, $p > 0.05$, $n = 4$ cells) and HVA Ca_V channel currents (19 ± 12%, $p > 0.05$, $n = 3$ cells).

To investigate whether the weak block of Ca_V channels by rAps III was due to a shift in the threshold of Ca_V channel activation, the I_{Ba}-V relationship was examined. The I_{Ba}-V relationships were established from families of I_{Ba} generated by 100-ms depolarising test potentials from V_h of −90 mV to +40 mV, at 5-mV increments every 7 s. Families of peak inward I_{Ba} were normalised against the maximum control inward peak I_{Ba} and plotted against the membrane potential (Fig. 5Ba). Ca_V channels activated around −60 mV, and this threshold was not altered in the presence of 1 μM rAps III. Additionally, there were no significant shifts in the $V_{1/2}$ of channel activation ($p > 0.05$, $n = 4$ cells) and currents were

essentially superimposable when normalised to the peak I_{Ba} (Fig. 5Bb). The partial block of Ca_V channels by rAps III was also voltage-independent ($p > 0.05$, $n = 4$ cells, data not shown).

3.6 rAps III does not modulate the activity of insect K_V channels

The major outward K_V channel current subtypes present in cockroach DUM neurons include a slowly activating, non-inactivating delayed-rectifier [$I_{K(DR)}$], transient "A-type" [$I_{K(A)}$], and large-conductance Ca^{2+}-activated [$I_{BK(Ca)}$] K_V channel currents [28, 50]. To determine the effects of 1 μM rAps III on K_V channels, global K_V channel currents (I_K) were generated by 100-ms depolarising test pulses to +25 mV from a V_h of −80 mV, every 5 s (0.2 Hz). This generated a large outward I_K that displayed fast activation and partial inactivation, consistent with global I_K previously observed in cockroach DUM neurons [27, 28]. Global I_K were measured at the peak and at the end of the test pulse (100 ms). The early peak global I_K results mainly from the contribution of rapidly activating $I_{K(A)}$ and $I_{K(Ca)}$, while the late global I_K results from the slowly activating $I_{K(DR)}$ and slow inactivating component of the $I_{K(Ca)}$.

Application of 1 μM rAps III caused minimal inhibition of global I_K. rAps III reduced the peak global I_K by only 2 ± 2% ($p > 0.05$, $n = 4$ cells; Fig. 5C) while late global I_K were inhibited only slightly by 5 ± 2% ($p < 0.05$, $n = 4$ cells; Fig. 5C). This lack of overt activity was mirrored by the lack of effect on the voltage-dependence of global I_K activation. Global I_K-V relationships for early and late currents were not significantly altered with no marked differences in $V_{1/2}$ values between the I_K-V for controls ($V_{1/2}$ = 3 mV for early and −4 mV for late I_K) versus toxin ($V_{1/2}$ = −4 mV for early and −9 mV for late I_K) (Fig. 5D). Due to the lack of any overt activity of 1 μM rAps III on global K_V channel currents, the effect of rAps III on individual K_V channel sub-types was not pursued. We conclude that rAps III does not modulate the activity of delayed-rectifier, 'A-type' or BK_{Ca} potassium channels that are the major contributors to the global outward K_v channel current in DUM neurons [51].

3.7 rAps III is a potent blocker of cloned cockroach Na_V channels

To further investigate the ability of rAps III to inhibit insect Na_V channels, we applied the toxin to *Xenopus* oocytes expressing the cloned $BgNa_V1$ channel [31]. At 1 μM concentration, rAps III strongly inhibited $BgNa_V1$-mediated sodium currents over a wide voltage range (Fig. 6A,B). Boltzmann fits of conductance-voltage relationships before ($V_{1/2}$ = −27 ± 1 mV; slope factor = 4.1 ± 0.2) and after ($V_{1/2}$ = −27 ± 1 mV; slope factor = 4.6 ± 0.3; $n = 3$ cells) toxin addition as well as the steady-state inactivation relationships (control: $V_{1/2}$ = −53 ± 1 mV; slope factor = 4.3 ± 0.1 and toxin: $V_{1/2}$ = −55 ± 1mV; slope factor = 4.3 ± 0.2; $n = 3$ cells) revealed no significant changes in the midpoints or slope factors (Fig. 6C). The onset of rAps III action is rapid, and there is a fast and complete recovery of channel current upon toxin washout (Fig. 6D). In contrast to gating-modifier toxins that inhibit channel opening by interacting with one or more of the four Na_V channel voltage sensors [52], rAps III decreased I_{Na} without shifting the midpoint of activation to more depolarised voltages (Fig. 6B). Together with the experiments reported above on DUM neurons (Fig. 3), this is consistent with a pore-blocking activity.

3.8 High-resolution solution structure of rAps III

The development of an efficient bacterial expression system allowed us to produce uniformly $^{13}C/^{15}N$-labelled rAps III for structure determination using heteronuclear NMR. ^1H_N, ^{15}N, $^{13}C_\alpha$, $^{13}C_\beta$, and $^{13}C'$ resonance assignments for the toxin were obtained from analysis of amideproton strips in 3D HNCACB, CBCA(CO)NH, and HNCO spectra. Sidechain ^1H and ^{13}C chemical shifts were obtained using a 4D HCC(CO)NH-TOCSY experiment, which has the advantage of providing sidechain ^1H-^{13}C connectivities [34].

Complete chemical shift assignments have been deposited in BioMagResBank (Accession Number 18946).

CYANA was used for automated NOESY assignment and structure calculation [38]. The disulfide-bond pattern (1–4, 2–5, 3–8, 6–7; see Fig. 1B) was unambiguously determined from preliminary structures calculated without disulfide-bond restraints [53]; this disulfide framework is notably different from the 1–4, 2–5, 3–6, 7–8 framework predicted in the UniProt entry for rAps III (P49268). Disulfide-bond and hydrogen-bond restraints were used in the final round of structure calculations. 200 structures were calculated from random starting conformations, then the 20 conformers with highest stereochemical quality as judged by MolProbity [54] were selected to represent the solution structure of rAps III. Coordinates for the final ensemble of structures are available from the Protein Data Bank (Accession Number 2M36).

Statistics highlighting the high precision and stereochemical quality of the ensemble of rAps III structures are shown in Table 1. The average MolProbity score of 1.67 places the ensemble in the 90th percentile relative to all other structures ranked by MolProbity. The high stereochemical quality of the ensemble stems from a complete absence of bad close contacts, very few unfavourable sidechain rotamers (5%), and reasonably high Ramachandran plot quality (85% of residues in the most favoured region). The structural ensemble is also highly precise with backbone and heavy-atom RMSD values over all residues of 0.32 ± 0.09 Å and 0.54 ± 0.07 Å, respectively. The ensemble of rAps III structures ranks as “high resolution” based on these measures of precision and stereochemical quality [55].

Fig. 7A shows a backbone overlay of the ensemble of 20 rAps III structures, while a schematic of the top-ranked structure highlighting key secondary structure elements is shown in Fig. 7B. Three of the four disulfide bonds in rAps III form a classical ICK motif in which the Cys2–16 and Cys9–20 disulfide bonds and the intervening sections of polypeptide backbone form a 13-residue ring that is pierced by the Cys15–Cys36 disulfide bond (Fig. 7A). This region forms a highly structured, disulfide-rich core from which emerges an unusual β-hairpin with a very large hairpin loop (Fig. 7B). The two β-strands of the hairpin are formed by residues 19–21 (β2) and 34–37 (β3), while the loop comprises residues 22–33. Residues 7–9 form a third β-strand (β1) and residues 11–14 form a single turn of 3_{10}-helix (α1) (Fig. 7B). A summary of the secondary structure of rAps III as judged by PDBsum [56] is shown in Fig. 7C.

While the compact ICK region of the rAps III structure is similar to previously determined structures of knottin peptides [57], the protruding β-hairpin loop, which often houses the pharmacophore in this class of spider toxins [15], is highly unusual. First, this hairpin is unusually large, comprising 13 residues (Fig. 7A,B). In comparison, the average size of the β-hairpin loop in the 35 spider-venom ICK toxins listed in ArachnoServer [17, 18] is 4.8 ± 1.8 residues. Second, the hairpin loop contains a glycine triplet (Gly29–Gly30–Gly31; underlined in Fig. 1B) that is rare in this class of toxins. Third, the glycine-rich portion of the loop is poorly defined in the ensemble of rAps II structures (Fig. 7A). Gly30 and to a lesser extent Gly32 consistently fall into unfavorable regions of the Ramachandran plot, suggesting that this region is highly dynamic in solution. Nevertheless, the dynamics of the triglycine loop is likely to be limited by the Cys27–Cys32 disulfide bond (Fig. 7A,B) which forms a molecular staple that serves to isolate this loop from the remainder of the β-hairpin, which in contrast is well structured.

It should be noted that the disulfide framework has not been experimentally established for native Aps III. However, the fact that rAps III is insecticidal and that it contains an ICK

motif that is the defining structural characteristic of this class of toxins suggests that the recombinant peptide has the same disulfide framework and 3D fold as the native peptide.

4. DISCUSSION

4.1 rAps III potently inhibits insect Na_V channels

In the present study, the effect of recombinantly produced Aps III was examined on three families of insect voltage-activated ion channels: Na_V, Ca_V and K_V channels. The main effect of rAps III was to produce a concentration-dependent inhibition of insect Na_V channels with an estimated IC_{50} of 540 nM. The pharmacological properties of rAps III resemble those of 'pore blocking' toxins that target Na_V channels such as the guanidinium compounds TTX and saxitoxin as well as μ-conotoxins from marine cone snail venoms that reduce peak I_{Na} [58].

rAps III displays similar activity to μ-TRTX-Hhn2b (hainantoxin-I) and μ-TRTX-Hh1a (huwentoxin-III), depressant neurotoxins from the venom of the Chinese tarantulas *Haplopelma hainanum* and *H. huwenum*, respectively. These toxins have been postulated to block insect Na_V channels via binding to neurotoxin receptor site-1 near the mouth of the channel [59, 60]. Both toxins block insect Na_V channels more potently than vertebrate Na_V channels. For example, μ-TRTX-Hhn2b blocks *Drosophila melanogaster* Na_V channels expressed in *Xenopus* oocytes with an IC_{50} of 4.5 μM compared with a 15-fold higher IC_{50} of 68 ± 6 μM for block of rat $Na_V1.2$ channels [59]. μ-TRTX-Hh1a did not block any of the vertebrate Na_V channel subtypes expressed in rat dorsal root ganglion neurons but it inhibited insect Na_V channel currents in cockroach DUM neurons with an IC_{50} of 1.1 μM [60]. Thus, although both μ-TRTX-Hhn2b and μ-TRTX-Hh1a selectively block insect Na_V channels, rAps III targets the insect channel with higher affinity, consistent with its high level of lethality (LD_{50} = 133 pmol/g) in larvae of the tobacco hornworm *Manduca sexta* [16].

One mechanism that can lead to inhibition of I_{Na} is an increase in the number of Na_V channels stabilised in the inactivated state. μ-TMTX-Hme1a (Hm-1) from the venom of the spider *Heriaeus melloteei* inhibits mammalian Na_V channels expressed in *Xenopus* oocytes without an alteration in the activation or inactivation kinetics of the channel [61]. The reduction in peak I_{Na} produced by μ-TMTX-Hme1a results from a shift in steady-state Na_V channel inactivation in the hyperpolarising direction [61]. Thus, the number of closed channels available for opening is reduced, resulting in flaccid paralysis. Unlike μ-TMTX-Hme1a, neither rAps III nor μ-TRTX-Hh1a produce a significant shift in the voltage-dependence of steady-state Na_V channel inactivation. Thus rAps III does not share a common mode of action with μ-TMTX-Hme1a, despite its ability to inhibit I_{Na}.

Interestingly, rAps III displays weak sequence homology with a range of spider δ-toxins (41% homology). All δ-toxins are gating modifiers that delay Na_V channel inactivation via an interaction with the voltage sensor of channel domain IV [62–67]. As a result, cells generate spontaneous and repetitive action potentials at, or near, the resting membrane potential to induce contractile paralysis [65]. A similar effect has been noted with spider β-toxins that shift the voltage-dependence of activation in the hyperpolarising direction primarily via an interaction with the voltage sensor of channel domain II [52, 68, 69]. However, the lack of any significant shifts in the voltage-dependence of Na_V channel activation or slowing of Na_V channel inactivation kinetics indicates that the effect of rAps III on Na_V channels is not due a modification of channel gating. Other toxins, such as the depressant toxin β-TRTX-Cm1a (ceratotoxin-1) from the straight-horned tarantula *Ceratogyrus marshalli*, can inhibit I_{Na} by shifting the voltage dependence of activation in the *depolarising* direction to produce a depressant phenotype [70]. In contrast, rAps III

inhibits insect Na_V channels conductance in the absence of any depolarising shift in the voltage-dependence of activation. In summary, rAps III does not cause a hyperpolarising shift (as seen for excitatory spider β-toxins) or a depolarising shift (as observed for depressant spider β-toxins) in the voltage-dependence of Na_V channel activation, nor does it slow the kinetics of Na_V channel inactivation as observed for spider δ-toxins.

Based on the pharmacology described here, Aps III should be renamed μ-cyrtautoxin-As1a (μ-CUTX-As1a) based on the rational nomenclature recently proposed for spider-venom peptides [71]. This is consistent with its action to induce flaccid paralysis in *M. sexta* by inhibiting neuronal excitability [16], in contrast with the spastic paralysis observed with δ-toxins and excitatory β-toxins.

4.2 Promiscuous activity of rAps III on insect Na_V and Ca_V channels

While rAps III inhibits insect Na_V channels with higher potency than other insect-selective spider neurotoxins such as μ-TRTX-Hhn2b and μ-TRTX-Hh1a, the IC_{50} value (540 nM) is still relatively high compared to spider toxins that inhibit vertebrate Na_V channels [45]. This suggests that rAps III may also target other voltage-activated channels. Spider toxins can interact with more than one target often across voltage-activated ion channel families and/or across channel subtypes to elicit multiple functions. This non-selective activity is due to the common structural elements shared between voltage-activated ion channels that are recognised by these toxins [72]. Na_V and Ca_V channels, in particular, are closely related and contain shared structural motifs and functional domains. Thus it is not surprising to find toxins with promiscuous activity across these channel families [49, 67]. Promiscuous activity of spider toxins with high affinity for both Na_V and K_V, or Na_V and Ca_V, channels is not without precedence and has been previously demonstrated by vertebrate active spider toxins including the NaV/KV channel toxins μ/ω-TRTX-Hh1a [73] and β/κ-TRTX-Cj1a [74] and the NaV/CaV channel toxin β/ω-TRTX-Tp2a (ProTx-II) [75]. Moreover, spider toxins targeting Ca_V channels with additional low affinity for Na_V channels have also been described including ω-TRTX-Hg1a (SNX482) [76], ω-agatoxin-Aa4a (ω-Aga-IVA)[77] and ω-hexa-toxin-Ar1a[46].

In addition to its effect on Na_V channels, 1 μM rAps III produced a modest 30% block of M-LVA and HVA Ca_V channel currents without any change in the voltage-dependence of Ca_V channel activation or inactivation kinetics. Most spider ω-toxins block M-LVA and HVA Ca_V channels in DUM neurons with IC_{50} values in the range 270–1000 nM (Table 2). Thus, Ca_V channels are unlikely to be the primary target of rAps III, but this pharmacology might contribute to the depressant phenotype by blocking Ca^{2+} entry into nerve terminals and thus inhibiting excitatory neurotransmitter release.

4.3 Advantages of complementary pharmacologies

rAps III produces marked inhibition of Na_V channels to inhibit action potential generation and propagation as well as partial block of Ca_V channels to inhibit neurotransmitter release. Both of these pharmacological sensitivities would cause inhibition of neurotransmission, consistent with the flaccid paralysis induced by rAps III in insect toxicity assays. While the inhibition of Ca_V channels by rAps III is not as potent as other spider ω-toxins with highly selective actions on a single target, the combined inhibition of both Na_V and both Ca_V channel subtypes by rAps III is likely responsible for its potent insecticidal activity. It should be noted that insects have a much smaller repertoire of Ca_V channels than vertebrates, with only a single ortholog of the vertebrate Ca_V1, Ca_V2 and Ca_V3 subtypes [48]. Thus, even moderate inhibition of Ca_V channels can be lethal to insects [48].

4.4 The unusual structure of rAps III might contribute to its novel pharmacology

In addition to its novel mode of action, the 3D structure of rAps III diverges significantly from typical spider-venom ICK toxins in that it contains an unusually large β-hairpin loop. The upper portion of this loop is stapled together by an additional disulfide bridge that serves to limit the solution dynamics of the unusual triglycine region of the loop. Although additional studies will be required to determine the precise mechanism of action and binding site of rAps III on insect Na_V channels, the current data suggests that it might bind in the outer vestibule of the channel rather than interact with one of the voltage-sensor domains. The large β-hairpin loop increases the footprint of this region of the toxin compared with other ICK-containing spider-venom toxins, and computer modelling (E. Deplazes and G.F. King, unpublished) indicates that the β-hairpin loop is an ideal size to fit into the turret region of the recently determined crystal structures of bacterial Na_V channels [78]. Thus, in addition to being a useful bioinsecticide lead, rAps III might prove to be a valuable pharmacological tool for the study of invertebrate Na_V channels.

Acknowledgments

We thank Ke Dong (Michigan State University) for the BgNav1 and TipE clones, Geoff Brown (Department of Agriculture, Fisheries and Forestry, Brisbane) for the supply of blowflies, and the Queensland NMR Network for access to the 900 MHz NMR spectrometer at the University of Queensland. This work was supported by grants from the Australian Research Council (Discovery Grant DP1095728 to G.F.K.) and the National Institute of Neurological Disorders And Stroke of the National Institutes of Health (Award Number R00NS073797 to F.B.).

References

1. Tedford HW, Sollod BL, Maggio F, King GF. Australian funnel-web spiders: master insecticide chemists. Toxicon. 2004; 43:601–618. [PubMed: 15066416]
2. World Health Organization. World Malaria Report. Geneva, Switzerland: WHO Press; 2009.
3. Oerke EC. Crop losses to pests. J Agric Sci. 2006; 144:31–43.
4. Pimental, D. Pesticides and pest control. In: Peshin, R.; Dhawan, AK., editors. Integrated pest management: innovation-development process. Dordrecht: Springer Verlag; 2009. p. 83-87.
5. Tedford HW, Gilles N, Ménez A, Doering CJ, Zamponi GW, King GF. Scanning mutagenesis of ω-atracotoxin-Hv1a reveals a spatially restricted epitope that confers selective activity against invertebrate calcium channels. J Biol Chem. 2004; 279:44133–44140. [PubMed: 15308644]
6. Bass C, Field LM. Gene amplification and insecticide resistance. Pest Manag Sci. 2011; 67:886–890. [PubMed: 21538802]
7. King GF, Hardy MC. Spider-venom peptides: structure, pharmacology, and potential for control of insect pests. Annual review of entomology. 2013; 58:475–496.
8. Gatehouse AM, Ferry N, Edwards MG, Bell HA. Insect-resistant biotech crops and their impacts on beneficial arthropods. Philos Trans R Soc Lond B – Biol Sci. 2011; 366:1438–1452. [PubMed: 21444317]
9. Bates SL, Zhao JZ, Roush RT, Shelton AM. Insect resistance management in GM crops: past, present and future. Nat Biotechnol. 2005; 23:57–62. [PubMed: 15637622]
10. Maggio, F.; Sollod, BL.; Tedford, HW.; Herzig, V.; King, GF. Spider toxins and their potential for insect control. In: LI, G.; Gill, SS., editors. Insect Pharmacology: Channels, Receptors, Toxins and Enzymes. London: Academic Press; 2010. p. 101-123.
11. Kuhn-Nentwig, L.; Stöcklin, R.; Nentwig, W. Venom composition and strategies in spiders: is everything possible?. Casas, J., editor. Elsevier: Spider Physiology and Behaviour—Physiology; 2011. p. 1-86.
12. Windley MJ, Herzig V, Dziemborowicz SA, Hardy MC, King GF, Nicholson GM. Spider-venom peptides as bioinsecticides. Toxins. 2012; 4:191–227. [PubMed: 22741062]
13. Pallaghy PK, Nielsen KJ, Craik DJ, Norton RS. A common structural motif incorporating a cystine knot and a triple-stranded β-sheet in toxic and inhibitory polypeptides Protein Sci. 1994; 3:1833–1839.

14. King GF, Tedford HW, Maggio F. Structure and function of insecticidal neurotoxins from Australian funnel-web spiders. J Toxicol Toxin Rev. 2002; 21:359–389.
15. Saez NJ, Senff S, Jensen JE, Er SY, Herzig V, Rash LD, et al. Spider-venom peptides as therapeutics. Toxins. 2010; 2:2851–2871. [PubMed: 22069579]
16. Skinner WS, Dennis PA, Li JP, Quistad GB. Identification of insecticidal peptides from venom of the trap-door spider, Aptostichus schlingeri (Ctenizidae). Toxicon. 1992; 30:1043–1050. [PubMed: 1440641]
17. Wood DL, Miljenovic T, Cai S, Raven RJ, Kaas Q, Escoubas P, et al. ArachnoServer: a database of protein toxins from spiders. BMC Genomics. 2009; 10:375. [PubMed: 19674480]
18. Herzig V, Wood DLA, Newell F, Chaumeil PA, Kaas Q, Binford GJ, et al. ArachnoServer 2.0, an updated online resource for spider toxin sequences and structures Nucleic Acids Res. 2011; 39:D653–D657.
19. Klint JK, Senff S, Rupasinghe DB, Er SY, Herzig V, Nicholson GM, et al. Spider-venom peptides that target voltage-gated sodium channels: pharmacological tools and potential therapeutic leads. Toxicon. 2012; 60:478–491. [PubMed: 22543187]
20. Fang L, Jia KZ, Tang YL, Ma DY, Yu M, Hua ZC. An improved strategy for high-level production of TEV protease in Escherichia coli and its purification and characterization. Protein expression and purification. 2007; 51:102–109. [PubMed: 16919473]
21. Cabrita LD, Dai W, Bottomley SP. A family of E. coli expression vectors for laboratory scale and high throughput soluble protein production. BMC Biotechnol. 2006; 6:12. [PubMed: 16509985]
22. Bassford JP. Export of the periplasmic maltose-binding protein of Escherichia coli. J Bioenerg Biomembr. 1990; 22:401–439. [PubMed: 2202725]
23. Kapust RB, Waugh DS. Escherichia coli maltose-binding protein is uncommonly effective at promoting the solubility of polypeptides to which it is fused. Protein Sci. 1999; 8:1668–1674. [PubMed: 10452611]
24. Saez NJ, Mobli M, Bieri M, Chassagnon IR, Malde AK, Gamsjaeger R, et al. A dynamic pharmacophore drives the interaction between psalmotoxin-1 and the putative drug target acid-sensing ion channel 1a. Mol Pharmacol. 2011; 80:796–808. [PubMed: 21825095]
25. Eitan M, Fowler E, Herrmann R, Duval A, Pelhate M, Zlotkin E. A scorpion venom neurotoxin paralytic to insects that affects sodium current inactivation: purification, primary structure, and mode of action. Biochemistry. 1990; 29:5941–5947. [PubMed: 2383565]
26. Herzig V, Hodgson WC. Neurotoxic and insecticidal properties of venom from the Australian theraphosid spider Selenotholus foelschei. Neurotoxicology. 2008; 29:471–475. [PubMed: 18423874]
27. Gunning SJ, Maggio F, Windley MJ, Valenzuela SM, King GF, Nicholson GM. The Janus-faced atracotoxins are specific blockers of invertebrate K_{ca} channels. FEBS J. 2008; 275:4045–4059. [PubMed: 18625007]
28. Windley MJ, Escoubas P, Valenzuela SM, Nicholson GM. A novel family of insect-selective peptide neurotoxins targeting insect large-conductance calcium-activated K^+ channels isolated from the venom of the theraphosid spider Eucratoscelus constrictus. Mol Pharmacol. 2011; 80:1–13. [PubMed: 21447641]
29. Barry PH. JPCalc, a software package for calculating liquid junction potential corrections in patch-clamp, intracellular, epithelial and bilayer measurements and for correcting junction potential measurements. J Neurosci Methods. 1994; 51:107–116. [PubMed: 8189746]
30. Wicher D, Penzlin H. Ca^{2+} currents in central insect neurons: electrophysiological and pharmacological properties. J Neurophysiol. 1997; 77:186–199. [PubMed: 9120560]
31. Tan J, Liu Z, Nomura Y, Goldin AL, Dong K. Alternative splicing of an insect sodium channel gene generates pharmacologically distinct sodium channels. J Neurosci. 2002; 22:5300–5309. [PubMed: 12097481]
32. Feng G, Deak P, Chopra M, Hall LM. Cloning and functional analysis of TipE, a novel membrane protein that enhances Drosophila para sodium channel function. Cell. 1995; 82:1001–10011. [PubMed: 7553842]
33. Zhou W, Goldin AL. Use-dependent potentiation of the $Na_V1.6$ sodium channel. Biophys J. 2004; 87:3862–3872. [PubMed: 15465873]

34. Mobli M, Stern AS, Bermel W, King GF, Hoch JC. A non-uniformly sampled 4D HCC(CO)NH-TOCSY experiment processed using maximum entropy for rapid protein sidechain assignment. J Magn Reson. 2010; 204:160–164. [PubMed: 20299257]
35. Mobli M, Maciejewski MW, Gryk MR, Hoch JC. An automated tool for maximum entropy reconstruction of biomolecular NMR spectra. Nat Meth. 2007; 4:467–468.
36. Shen Y, Delaglio F, Cornilescu G, Bax A. TALOS+: a hybrid method for predicting protein backbone torsion angles from NMR chemical shifts. J Biomol NMR. 2009; 44:213–223. [PubMed: 19548092]
37. Fletcher JI, Smith R, O'Donoghue SI, Nilges M, Connor M, Howden MEH, et al. The structure of a novel insecticidal neurotoxin, ω-atracotoxin-HV1, from the venom of an Australian funnel web spider. Nat Struct Biol. 1997; 4:559–566. [PubMed: 9228949]
38. Güntert P. Automated NMR structure calculation with CYANA. Methods Mol Biol. 2004; 278:353–378. [PubMed: 15318003]
39. Vetter I, Davis JL, Rash LD, Anangi R, Mobli M, Alewood PF, et al. Venomics: a new paradigm for natural products-based drug discovery. Amino Acids. 2011; 40:15–28. [PubMed: 20177945]
40. Meng E, Cai TF, Li WY, Zhang H, Liu YB, Peng K, et al. Functional expression of spider neurotoxic peptide huwentoxin-I in E. coli. PLoS One. 2011; 6:e21608. [PubMed: 21731778]
41. Heras B, Shouldice SR, Totsika M, Scanlon MJ, Schembri MA, Martin JL. DSB proteins and bacterial pathogenicity. Nat Rev Microbiol. 2009; 7:215–225. [PubMed: 19198617]
42. Sackett, D.; Holmes, P.; Abbott, K.; Jephcott, S.; Barber, M. Assessing the economic cost of endemic disease on the profitability of Australian beef cattle and sheep producers. Sydney: Meat & Livestock Australia; 2006.
43. Vassilevski A, Kozlov S, Grishin E. Molecular diversity of spider venom. Biochemistry (Moscow). 2009; 74:1505–1534. [PubMed: 20210706]
44. Bosmans, F.; Escoubas, P.; Nicholson, GM. Spider venom peptides as leads for drug and insecticide design. In: de Lima, ME.; Pimenta, AMC.; Martin-Eauclaire, MF.; Zingali, RB.; Rochat, H., editors. Animal Toxins: State of the Art Perspectives In Health and Biotechnology. Belo Horizonte: Federal University of Minas Gerais Press; 2009. p. 269-290.
45. Yamaji N, Little MJ, Nishio H, Billen B, Villegas E, Nishiuchi Y, et al. Synthesis, solution structure, and phylum selectivity of a spider δ-toxin that slows inactivation of specific voltage-gated sodium channel subtypes. J Biol Chem. 2009; 284:24568–24582. [PubMed: 19592486]
46. Chong Y, Hayes JL, Sollod B, Wen S, Wilson DT, Hains PG, et al. The ω-atracotoxins: selective blockers of insect M-LVA and HVA calcium channels. Biochemical pharmacology. 2007; 74:623–638. [PubMed: 17610847]
47. Zhang MM, Han TS, Olivera BM, Bulaj G, Yoshikami D. μ-conotoxin KIIIA derivatives with divergent affinities versus efficacies in blocking voltage-gated sodium channels. Biochemistry. 2010; 49:4804–4812. [PubMed: 20459109]
48. King GF. Modulation of insect Ca_V channels by peptidic spider toxins. Toxicon. 2007; 49:513–530. [PubMed: 17197008]
49. King GF, Escoubas P, Nicholson GM. Peptide toxins that selectively target insect Na_V and Ca_V channels. Channels. 2008; 2:100–116. [PubMed: 18849658]
50. Grolleau F, Lapied B. Separation and identification of multiple potassium currents regulating the pacemaker activity of insect neurosecretory cells (DUM neurons). J Neurophysiol. 1995; 73:160–171. [PubMed: 7714561]
51. Wicher D, Walther C, Wicher C. Non-synaptic ion channels in insects—basic properties of currents and their modulation in neurons and skeletal muscles. Prog Neurobiol. 2001; 64:431–525. [PubMed: 11301158]
52. Bosmans F, Swartz KJ. Targeting voltage sensors in sodium channels with spider toxins. Trends Pharmacol Sci. 2010; 31:175–182. [PubMed: 20097434]
53. Mobli M, King GF. NMR methods for determining disulfide-bond connectivities. Toxicon. 2010; 56:849–854. [PubMed: 20603141]
54. Davis IW, Leaver-Fay A, Chen VB, Block JN, Kapral GJ, Wang X, et al. MolProbity: all-atom contacts and structure validation for proteins and nucleic acids. Nucl Acids Res. 2007; 35:W375–W383. [PubMed: 17452350]

55. Kwan AH, Mobli M, Gooley PR, King GF, Mackay JP. Macromolecular NMR spectroscopy for the non-spectroscopist. FEBS J. 2011; 278:687–703. [PubMed: 21214860]
56. Laskowski RA. PDBsum new things. Nucleic Acids Res. 2009; 37:D355–D359. [PubMed: 18996896]
57. Gracy J, Le-Nguyen D, Gelly JC, Kaas Q, Heitz A, Chiche L. KNOTTIN: the knottin or inhibitor cystine knot scaffold in 2007. Nucleic Acids Res. 2008; 36:D314–D319. [PubMed: 18025039]
58. Shon KJ, Olivera BM, Watkins M, Jacobsen R, Gray WR, Floresca CZ, et al. μ-Conotoxin PIIIA, a new peptide for discriminating among tetrodotoxin-sensitive Na channel subtypes. J Neurosci. 1998; 18:4473–4481. [PubMed: 9614224]
59. Li D, Xiao Y, Hu W, Xie J, Bosmans F, Tytgat J, et al. Function and solution structure of hainantoxin-I, a novel insect sodium channel inhibitor from the Chinese bird spider Selenocosmia hainana. FEBS Lett. 2003; 555:616–622. [PubMed: 14675784]
60. Wang RL, Yi S, Liang SP. Mechanism of action of two insect toxins huwentoxin-III and hainantoxin-VI on voltage-gated sodium channels. J Zhejiang Univ Sci B. 2010; 11:451–457. [PubMed: 20506577]
61. Billen B, Vassilevski A, Nikolsky A, Tytgat J, Grishin E. Two novel sodium channel inhibitors from Heriaeus melloteei spider venom differentially interacting with mammalian channel's isoforms. Toxicon. 2008:309–317. [PubMed: 18606177]
62. Fletcher JI, Chapman BE, Mackay JP, Howden MEH, King GF. The structure of versutoxin (δ-atracotoxin-Hv1) provides insights into the binding of site 3 neurotoxins to the voltage-gated sodium channel. Structure. 1997; 5:1525–1535. [PubMed: 9384567]
63. Little MJ, Wilson H, Zappia C, Cestele S, Tyler MI, Martin-Eauclaire MF, et al. δ-atracotoxins from Australian funnel-web spiders compete with scorpion α-toxin binding on both rat brain and insect sodium channels. FEBS Lett. 1998:246–252. [PubMed: 9845331]
64. Little MJ, Zappia C, Gilles N, Connor M, Tyler MI, Martin-Eauclaire MF, et al. δ-Atracotoxins from Australian funnel-web spiders compete with scorpion a-toxin binding but differentially modulate alkaloid toxin activation of voltage-gated sodium channels. J Biol Chem. 1998; 273:27076–27083. [PubMed: 9765223]
65. Grolleau F, Stankiewicz M, Birinyi-Strachan L, Wang X, Nicholson GM, Pelhate M, et al. Electrophysiological analysis of the neurotoxic action of a funnel-web spider toxin, δ-atracotoxin-Hv1a, on insect voltage-gated Na^+ channels. J Exp Biol. 2001; 204:711–721. [PubMed: 11171353]
66. Matavel A, Cruz JS, Penaforte CL, Araujo DA, Kalapothakis E, Prado VF, et al. Electrophysiological characterization and molecular identification of the Phoneutria nigriventer peptide toxin PnTx2–6. FEBS Lett. 2002:523.
67. Nicholson GM. Insect-selective spider toxins targeting voltage-gated sodium channels. Toxicon. 2007; 49:490–512. [PubMed: 17223149]
68. Zeng X, Deng M, Lin Y, Yuan C, Pi J, Liang S. Isolation and characterization of Jingzhaotoxin-V, a novel neurotoxin from the venom of the spider Chilobrachys jingzhao. Toxicon. 2007; 49:388–399. [PubMed: 17157888]
69. Bosmans F, Martin-Eauclaire MF, Swartz KJ. Deconstructing voltage sensor function and pharmacology in sodium channels. Nature. 2008; 456:202–208. [PubMed: 19005548]
70. Bosmans F, Rash L, Zhu S, Diochot S, Lazdunski M, Escoubas P, et al. Four novel tarantula toxins as selective modulators of voltage-gated sodium channel subtypes. Mol Pharmacol. 2006; 69:419–429. [PubMed: 16267209]
71. King GF, Gentz MC, Escoubas P, Nicholson GM. A rational nomenclature for naming peptide toxins from spiders and other venomous animals. Toxicon. 2008; 52:264–276. [PubMed: 18619481]
72. Li-Smerin Y, Swartz KJ. Gating modifier toxins reveal a conserved structural motif in voltage-gated Ca^{2+} and K^+ channels. Proc Natl Acad Sci USA. 1998; 95:8585–8589. [PubMed: 9671721]
73. Wang M, Guan X, Liang S. The cross channel activities of spider neurotoxin huwentoxin-I on rat dorsal root ganglion neurons. Biochem Biophys Res Commun. 2007; 357:579–583. [PubMed: 17451655]

74. Liao Z, Yuan C, Peng K, Xiao Y, Liang S. Solution structure of Jingzhaotoxin-III, a peptide toxin inhibiting both $Na_v1.5$ and $K_v2.1$ channels. Toxicon. 2007; 50:135–143. [PubMed: 17481690]

75. Edgerton GB, Blumenthal KM, Hanck DA. Inhibition of the activation pathway of the T-type calcium channel $Ca_V3.1$ by ProTxII. Toxicon. 2010; 56:624–636. [PubMed: 20600227]

76. Arroyo G, Aldea M, Fuentealba J, Albillos A, García AG. SNX482 selectively blocks P/Q Ca^{2+} channels and delays the inactivation of Na^+ channels of chromaffin cells. Eur J Pharmacol. 2003; 475:11–18. [PubMed: 12954354]

77. Wicher D, Penzlin H. ω-Toxins affect Na^+ currents in neurosecretory insect neurons. Receptors & Channels. 1998; 5:355–366. [PubMed: 9826912]

78. Catterall WA. Voltage-gated sodium channels at 60: structure, function and pathophysiology. J Physiol. 2012; 590:2577–2589. [PubMed: 22473783]

79. Kubista H, Mafra RA, Nicholson GM, Beirão PS, Cruz JS, Boehm S, et al. CSTX-1, a toxin from the venom of the hunting spider *Cupiennius salei*, is a selective blocker of L-type calcium channels in mammalian neurons. Neuropharmacol. 2007; 52:1650–1662.

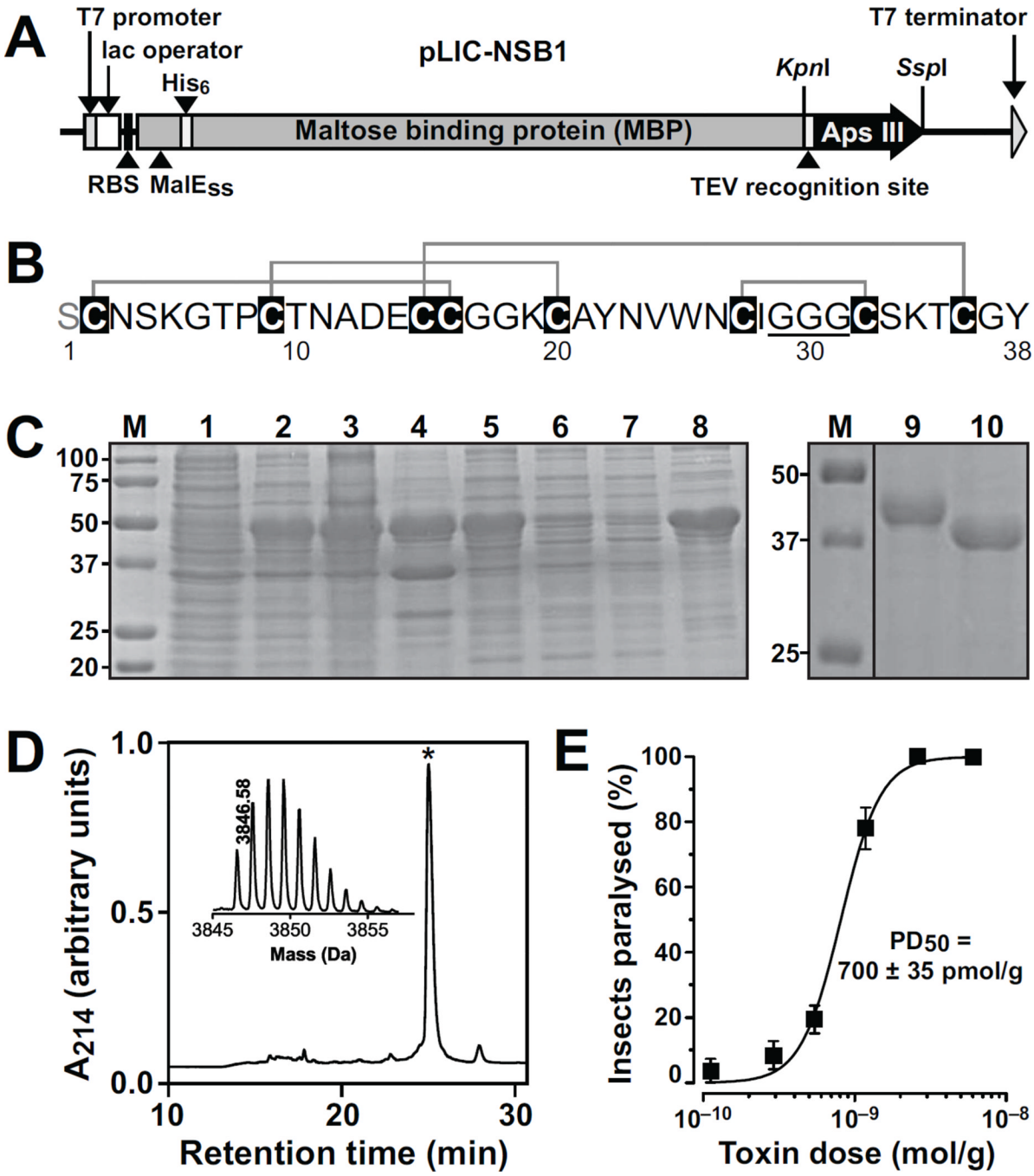

Fig. 1. Production and functional analysis of recombinant Aps III

(A) Schematic representation of the pLicC-NSB1 vector used for periplasmic expression of Aps III. The coding region includes a MalE signal sequence ($MalE_{SS}$) for periplasmic export, a His_6 affinity tag, an MBP fusion tag, and a codon-optimised gene encoding Aps III, with a TEV protease recognition site inserted between the MBP and toxin coding regions. The locations of key elements of the vector are shown, including the ribosome binding site (RBS). (**B**) Primary structure of rAps III. The non-native N-terminal Ser residue is highlighted in grey and the triglycine sequence is underlined. The disulfide framework of rAps III as determined in the current study is shown above the amino acid sequence. **(C)**

SDS-PAGE gels illustrating different steps in the purification of rAps III. Lanes are as follows: M, molecular weight markers; lane 1, *E. coli* cell extract prior to IPTG induction; lane 2, *E. coli* cell extract after IPTG induction; lane 3, lysate resulting from cell disruption; lane 4, soluble periplasmic extract; lane 5, Ni-NTA beads after loading the cell lysate (the His_6-MBP-Aps III fusion protein is evident at ~49 kDa); lane 6, eluate from washing Ni-NTA resin with loading buffer; lane 7, eluate from washing Ni-NTA resin with 10 mM imidazole; lane 8, eluate from washing Ni-NTA resin with 500 mM imidazole; lane 9, purified fusion protein before TEV cleavage; lane 10, fusion protein sample after TEV protease cleavage, showing complete cleavage of fusion protein to His_6-MBP. **(D)** RP-HPLC chromatogram showing the final step in the purification of rAps III. The asterisk denotes the peak corresponding to correctly folded rAps III. Inset is a MALDI-TOF MS spectrum showing the $[M+H]^+$ ion for the purified recombinant toxin (obs. = 3846.58 Da; calc. = 3846.49Da). **(E)** Dose-response curve for the paralytic effects of rAps III determined 24 h after injection into sheep blowflies (*L. cuprina*).

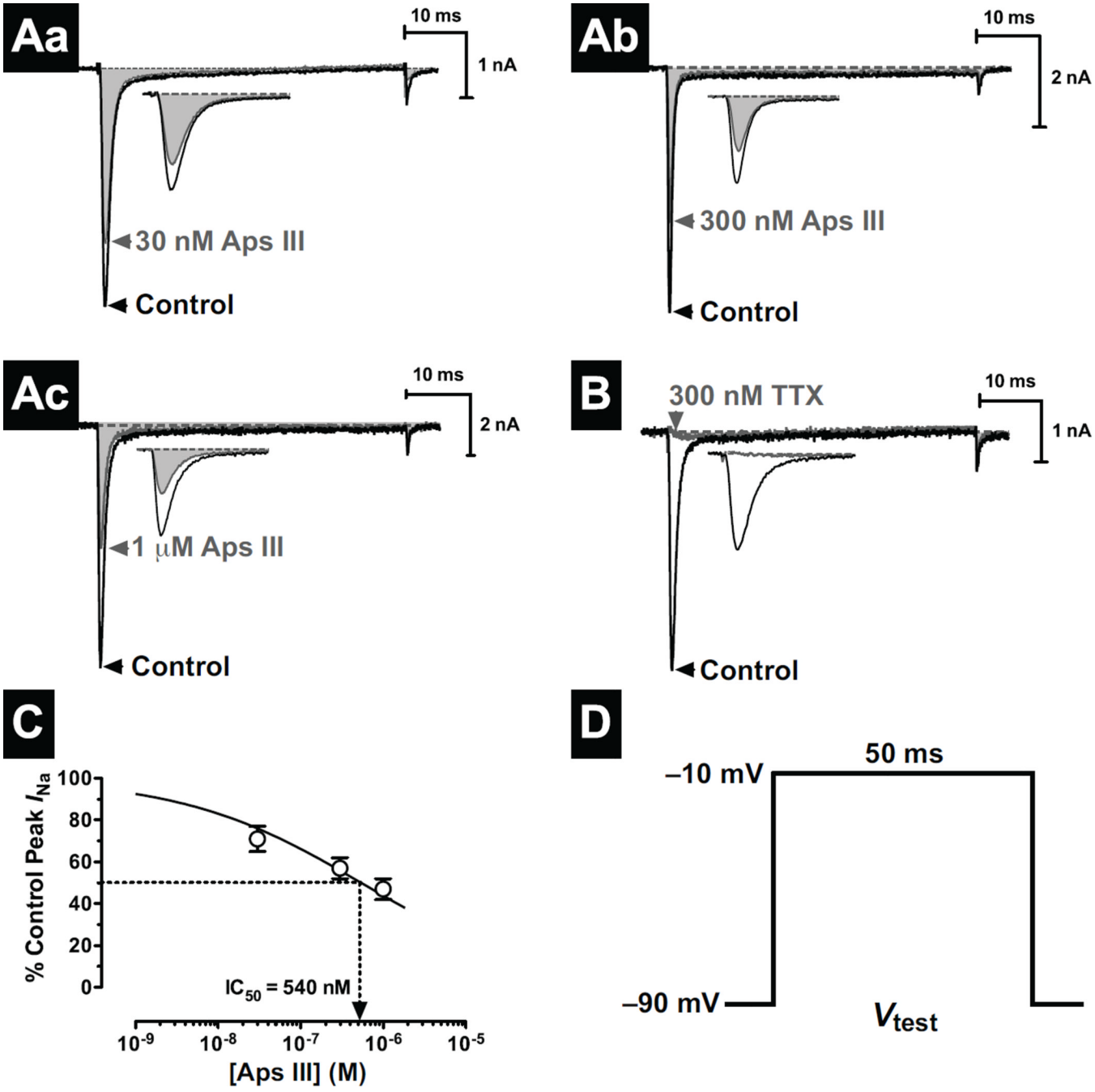

Fig. 2. Effects of rAps III on Na_V channels in cockroach DUM neurons

(Aa–c) Typical effects of increasing concentrations of rAps III on I_{Na}. Traces show superimposed control (black) and toxin (grey and shaded) current traces elicited by a 50-ms depolarising test pulse (V_{test}) shown in panel D. The reduction in I_{Na} is highlighted in the inset of panels Aa–c. **(B)** Complete block of I_{Na} by 300 nM TTX, confirming that ionic currents are solely mediated through Na_V channels. Dotted lines represent zero current. **(C)** Concentration-response relationship of rAps III to inhibit peak I_{Na}. The percentage block at increasing concentrations of rAps III were fitted with a logistic function (Eq. 1; see Materials and Methods). The median inhibitory concentration (IC_{50}) was determined to be 540 nM. Data points are the mean ± SEM of 5–9 cells.

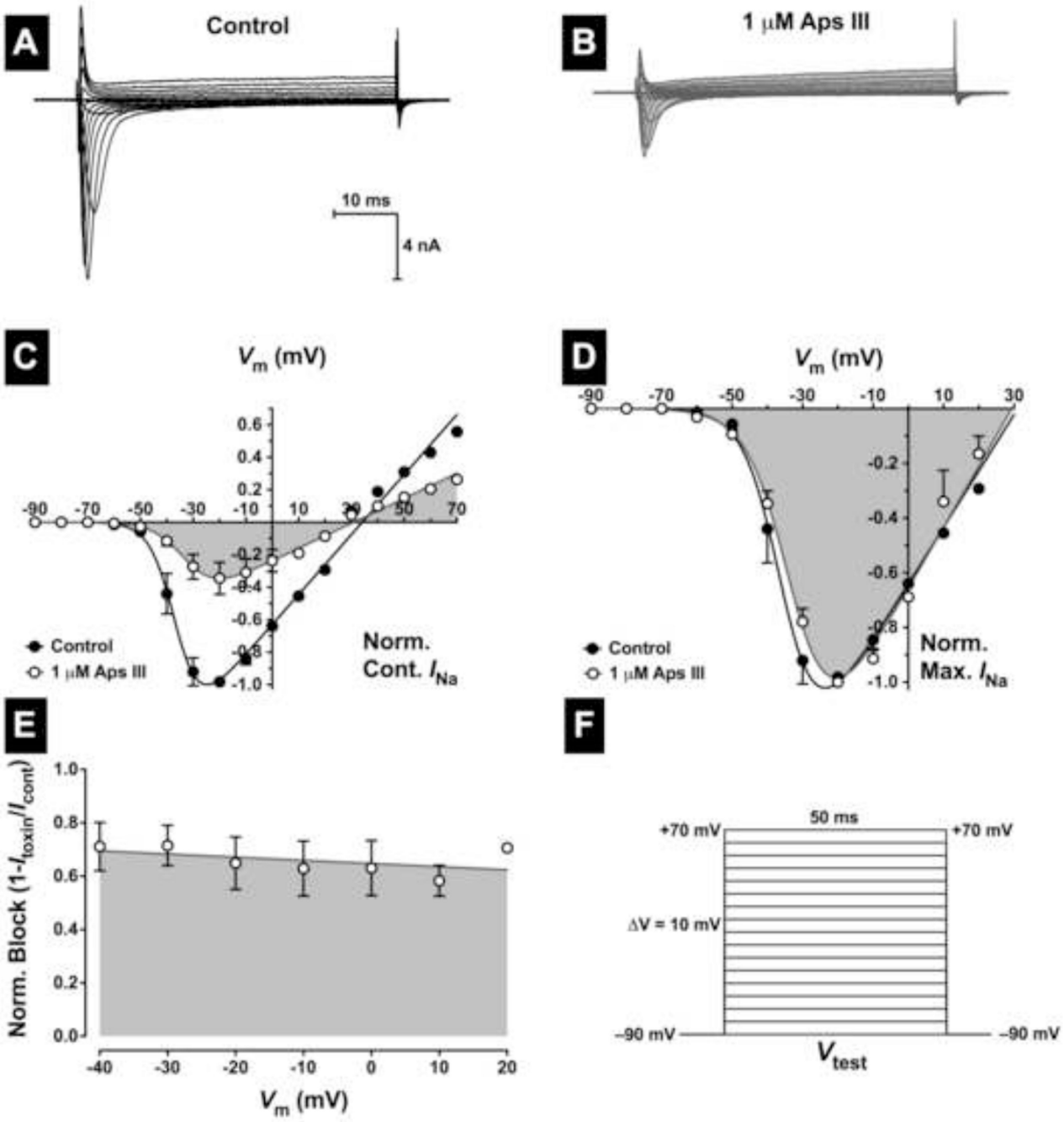

Fig. 3. Effects of rAps III on the voltage-dependence of Na_V channel activation in cockroach DUM neurons

Typical families of I_{Na} recorded prior to **(A)**, and following **(B)**, application of 1 μM rAps III. Nav channel currents were elicited by the test pulse protocol shown in panel **F. (C–D)** Normalised peak I_{Na}-V relationships. Currents recorded in the presence of 1 μM rAps III were normalised to the maximum inward I_{Na} in controls **(C)**, or maximum inward I_{Na} **(D)**. Data shows I_{Na} before (closed symbols), and after (open symbols and shaded), application of 1 μM rAps III. Data were fitted with Eq. 2 (see Materials and Methods). As can be seen in panel (**D**), no significant shifts in the voltage dependence of Na_V channel activation were observed. **(E)** Fractional block of I_{Na} by 1 μM rAps III showing lack of voltage dependence.

Normalised peak I_{Na} in the presence of toxin were calculated as a fraction of peak control I_{Na} and plotted against the test potential. Data were taken from panel C and fitted using linear regression. All data are expressed as the mean ± SEM of 4 cells.

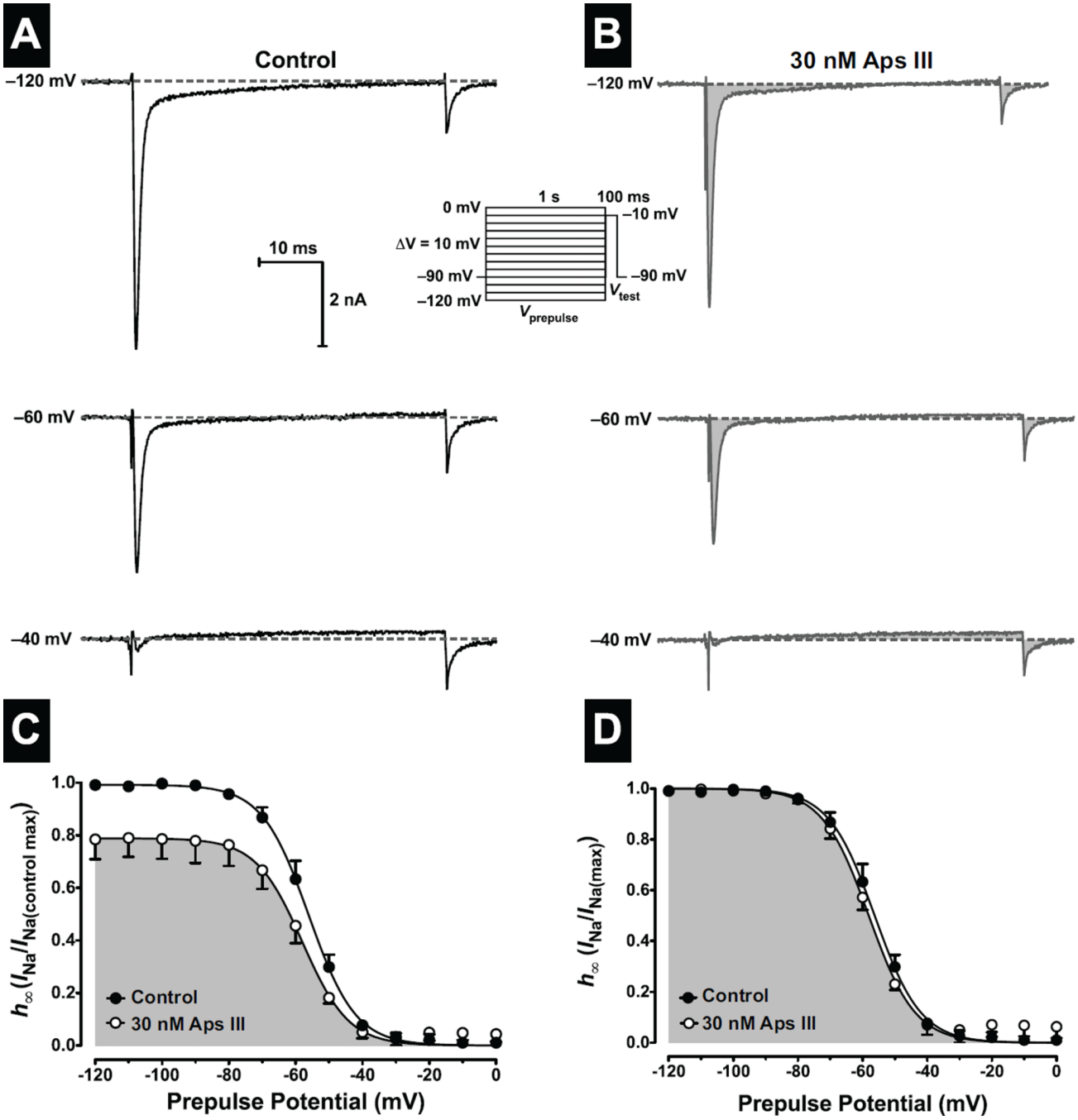

Fig. 4. Effects of rAps III on steady-state Na_V channel inactivation (h_∞)

Steady-state inactivation was determined using a two-pulse protocol (see inset). (**A–B**) Typical peak I_{Na} recorded during the test pulse (V_{test}) are shown following 1-s prepulse potentials ($V_{prepulse}$) to −120 mV, −60 mV and −40 mV recorded before (left-hand traces), and following (right-hand shaded traces), perfusion with 30 nM rAps III. Dotted lines represent zero current. (**C–D**) Peak I_{Na}, recorded during V_{test} were expressed as a fraction of maximum control I_{Na} (**C**), or normalised to peak I_{Na} amplitude (**D**), and plotted against prepulse potential. Panels show the proportion of I_{Na} that is available for activation under control conditions (closed circles), and during perfusion with 30 nM rAps III (open circles

and shaded). The h_{∞}/V curves were fitted with Eq. 3 (see Materials and Methods). All data are expressed as the mean ± SEM of 3 cells.

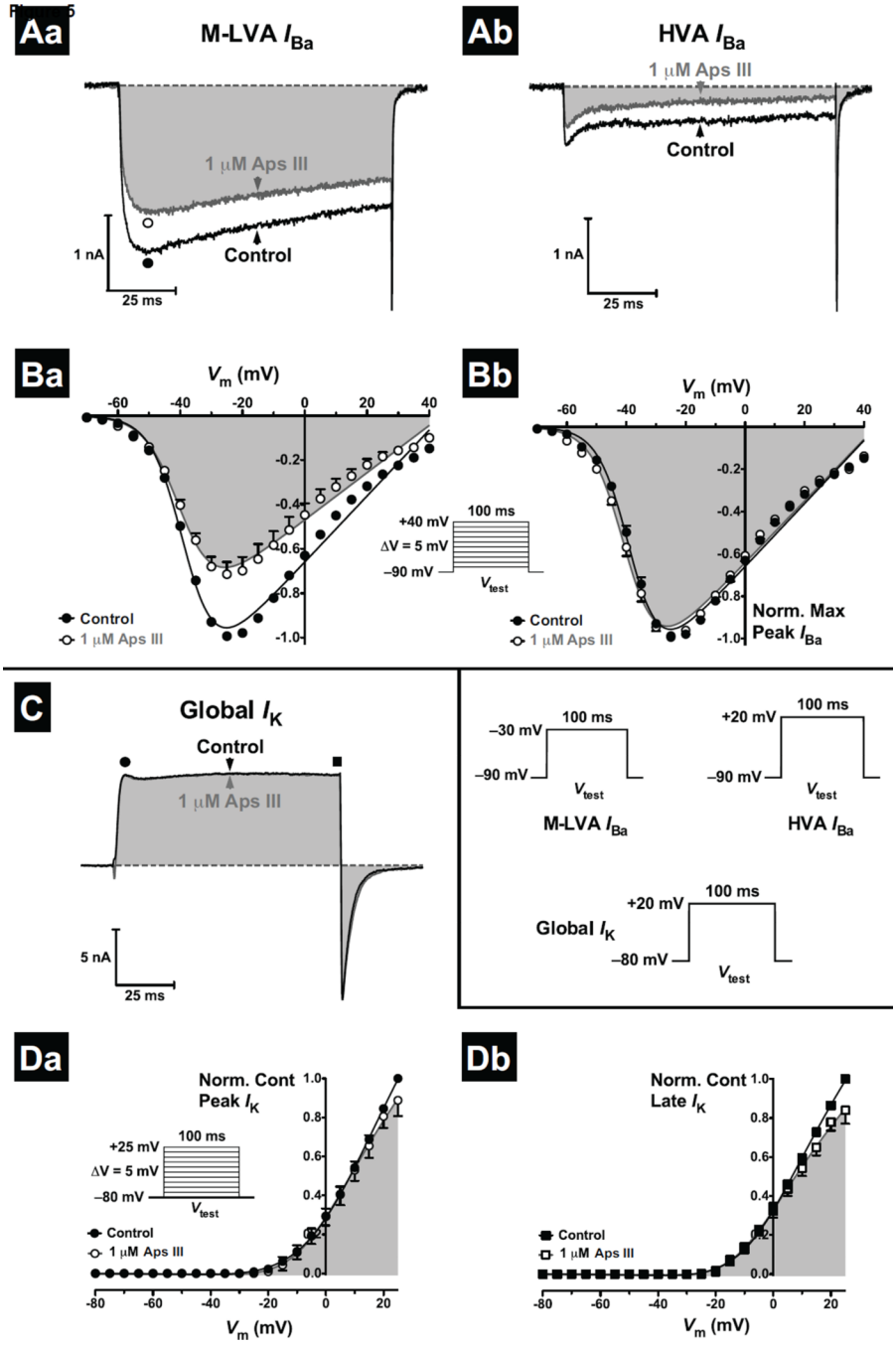

Fig. 5. Effect of rAps III on K_V and Ca_V channel currents in cockroach DUM neurons

(**A**) Whole-cell M-LVA and HVA I_{Ba} in the absence (black traces), and presence (dark grey and shaded traces), of 1 μM rAps III. M-LVA and HVA I_{Ba} were activated by a 100 ms V_{test} to −30 mV and +20 mV, respectively, as shown in the inset in panel C. Perfusion with 1 μM rAps III partially blocked M-LVA (**Aa**) and HVA (**Ab**) Ca_V channel currents. Dotted lines represent zero current. (**B**) Effects of 1 μM rAps III on the voltage-dependence of Ca_V channel activation. Families of Ca_V channel currents were generated by the V_{test} protocol shown in the inset of panel **C**. Currents recorded in the presence of 1 μM rAps III were normalised to the maximum inward I_{Ba} in control (**Ba**) or maximum inward I_{Ba} in toxin

(**Bb**). I_{Ba}-*V* relationships show current recorded before (closed circles), and after (open circles and shaded), perfusion with 1 μM rAps III. Normalised *I–V* relationships were fitted using Eq. 2. **(C)** Typical superimposed global I_K recorded prior to (black traces), and following (dark grey and shaded traces), application of 1 μM rAps III. Currents were generated by 100-ms depolarising test pulses (V_{test}) as shown in the as shown in the inset in panel C. (**D**) Effects of rAps III on the voltage-dependence of global K_V channel activation. Families of outward I_K were recorded before (closed circles), and after (open circles and shaded), application of 1 μM rAps III. Families of I_K were generated by the V_{test} protocol shown in the inset of panel **C**. Global I_K-*V* relationships show effects of the toxin on peak (**Da**) and late (**Db**) global I_K. Late currents were measured at 100 ms. All data are expressed as the mean ± SEM of 4 cells.

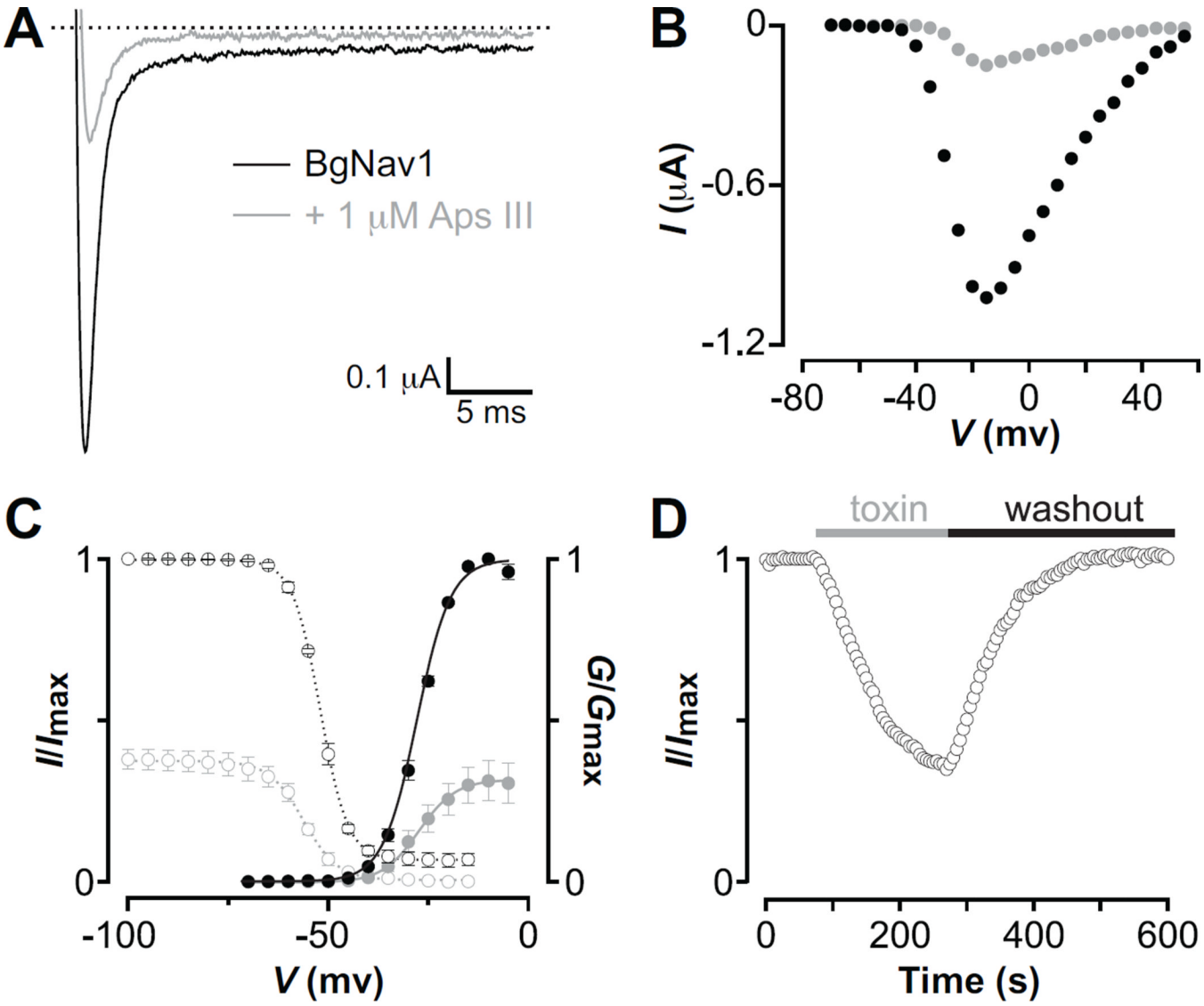

Fig. 6. rAps III inhibits BgNa$_V$1-mediated sodium currents

(A) Inhibition of BgNa$_V$1-mediated sodium currents by 1 μM rAps III at a depolarization to −20 mV from a holding voltage of −90 mV. **(B)** Representative I_{Na}-V relationship for BgNa$_V$1 before (black) and after (grey) addition of 1 μM rAps III. Currents were elicited by 5-mV step depolarizations from a holding voltage of −90 mV. **(C)** Comparison of the gating properties of BgNa$_V$1 before (black) and after (grey) addition of 1 μM rAps III. Shown are the deduced conductance (G)–voltage (filled circles) and steady-state inactivation (open circles) relationships. Error bars denote SEM, with n = 3 cells. **(D)** Onset of BgNa$_V$1-mediated I_{Na} inhibition by 1 μM rAps III at depolarizations to −20 mV (holding voltage was −90 mV) followed by a complete recovery after toxin washout.

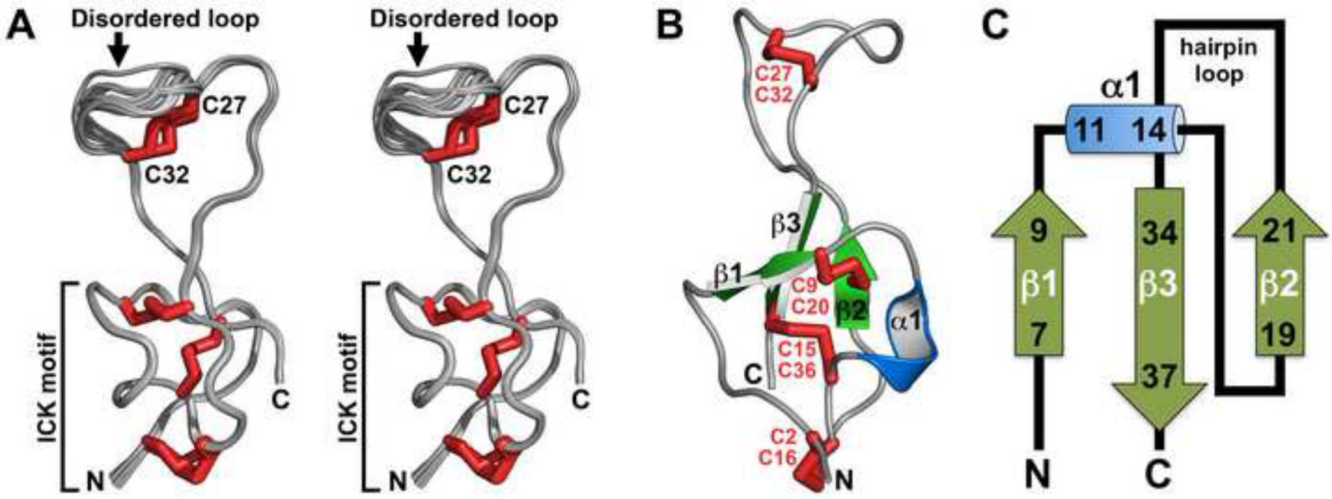

Fig. 7. Three-dimensional structure of rAps III

(A) Stereoview of an overlay of the ensemble of 20 rAps III structures. Disulfide bonds are highlighted in red and the N- and C-termini are labelled. The structures are overlaid over the backbone atoms of residues 2–27 and 32–38 in order to highlight the disordered nature of the triglycine loop (residues 27–32) relative to the well-structured ICK region of the toxin. **(B)** Ribbon representation of the rAps III structure highlighting the various secondary structure elements and disulfide bonds. The views in panels (B) and (C) are related by a ~180° rotation around the long axis of the molecule. **(C)** Topology map of the secondary structure of rAps III. The N- and C-termini are labelled.

Table 1

Structural statistics for the ensemble of rAps III structures.

Experimental restraints[2]		
Interproton distance restraints		
Intraresidue	111	
Sequential	159	
Medium range (i−j < 5)	93	
Long range (i−j ≥5)	165	
Hydrogen-bond restraints[3]	14	
Disulfide-bond restraints	12	
Dihedral-angle restraints (φ,ψ)	59	
Total number of restraints per residue		16.1
R.m.s. deviation from mean coordinate structure (Å)		
All backbone atoms (residues 1–38)	0.33 ± 0.08	
All heavy atoms (residues 1–38)	0.54 ± 0.07	
Backbone atoms (residues 2–27, 32–38)		0.13 ± 0.03
Heavy atoms (residues 2–27, 32–38)	0.43 ± 0.06	
Stereochemical quality[4]		
Residues in most favored Ramachandran region (%)	84.5 ± 2.8	
Ramachandran outliers (%)	2.4 ± 1.4	
Unfavorable sidechain rotamers (%)	5.0 ± 2.1	
Clashscore, all atoms[5]	0.0 ± 0.0	
Overall MolProbity score	1.67 ± 0.15	

[1] All statistics are given as mean ± S.D.

[2] Only structurally relevant restraints, as defined by CYANA, are included.

[3] Two restraints were used per hydrogen bond.

[4] According to MolProbity (http://molprobity.biochem.duke.edu)

[5] Defined as the number of steric overlaps >0.4 Å per thousand atoms

Table 2

Block of cockroach DUM neuron Ca_V channels by spider neurotoxins.

	Ca_V channel subtype		
Toxin	**M-LVA IC_{50} (nM)**	**HVA IC_{50} (nM)**	**Reference**
ω-HXTX-Hv1a	279	1080	[46]
ω-HXTX-Ar1a	692	644	[46]
ω-CNTX-Cs1a*	467	274	[79]

*Insecticidal toxin also active on mammalian Ca_V channels